There Is Communication between All Four Ca^{2+}-Bindings Sites of Calcineurin B†

Stephen C. Gallagher, Zhong-Hua Gao,‡ Shipeng Li,‡ R. Brian Dyer, Jill Trewhella,* and Claude B. Klee‡

Bioscience Division, Los Alamos National Laboratory, Los Alamos, New Mexico 87545, and Laboratory of Biochemistry, National Cancer Center Institute, National Institutes of Health, Bethesda, Maryland 20892-0520

Received October 30, 2000; Revised Manuscript Received June 1, 2001

ABSTRACT: We have used site-directed mutagenesis, flow dialysis, and Fourier transform infrared (FTIR) spectroscopy to study Ca^{2+}-binding to the regulatory component of calcineurin. Single Glu-Gln(E → Q) mutations were used to inactivate each of the four Ca^{2+}-binding sites of CnB in turn, generating mutants Q1, Q2, Q3, and Q4, with the number indicating which Ca^{2+} site is inactivated. The binding data derived from flow dialysis reveal two pairs of sites in the wild-type protein, one pair with very high affinity and the other with lower affinity Ca^{2+}-binding sites. Also, only three sites are titratable in the wild-type protein because one site cannot be decalcified. Mutation of site 2 leaves the protein with only two titratable sites, while mutation of sites 1, 3, or 4 leave three titratable sites that are mostly filled with 3 Ca^{2+} equiv added. The binding data further show that each of the single-site mutations Q2, Q3, and Q4 affects the affinities of at least one of the remaining sites. Mutation in either of sites 3 or 4 results in a protein with no high-affinity sites, indicating communication between the two high-affinity sites, most likely sites 3 and 4. Mutation in site 2 decreases the affinity of all three remaining sites, though still leaving two relatively high-affinity sites. The FTIR data support the conclusions from the binding data with respect to the number of titratable sites as well as the impact of each mutation on the affinities of the remaining sites. We conclude therefore that there is communication between all four Ca^{2+}-binding sites. In addition, the Ca^{2+} induced changes in the FTIR spectra for the wild-type and Q4 mutant are most similar, suggesting that the same three Ca^{2+}-binding sites are being titrated, i.e., site 4 is the very high-affinity site under the conditions of the FTIR experiments.

Calcineurin is a calcium- and calmodulin-dependent Ser/Thr protein phosphatase that is found in all eukaryotic cells (reviewed in ref *1*). It functions in T-cell activation and is a target for the immunosuppressive drugs cyclosporin and FK506 after they form complexes with the cytoplasmic binding proteins cyclophilin and FKBP12, respectively (*2*−*5*). The enzyme is made up of two tightly bound subunits: a 59 kDa component A (CnA)[1] containing the active site, and a 19.3 kDa component B (CnB) that provides regulatory control via Ca^{2+} binding. Additional regulatory control is exerted by the binding of Ca^{2+}/calmodulin to calcineurin. The regulatory CnB is closely related to calmodulin, although the proteins are not interchangeable and they bind to distinct sequence segments in CnA. Like calmodulin, CnB contains four helix-loop-helix [EF-hand] motifs (*6*−*8*). The Ca^{2+}-binding sites are of the all-oxygen coordinating type with pentagonal bipyramidal geometry (*7*), and they share high sequence homology with the Ca^{2+}-binding sites in calmodulin. The crystal structures of calcineurin complexed with FKBP12-FK506 (*7*, *8*) show that, as in calmodulin, the Ca^{2+}-binding sites of CnB occur in pairs forming two globular domains (termed the N- and C-domains), and there is a long C-terminal β-strand. The globular domains are connected via an α-helical segment that is strongly kinked at Gly85 such that they are brought into close contact and oriented to interact with the hydrophobic face of a helix in CnA. NMR data indicate that, when CnB is free in solution, residues 82−87 are flexible (*9*), similar to what was previously observed for the interconnecting helix region of calmodulin in solution (*10*, *11*).

In the wild-type calcineurin, one Ca^{2+} always remains bound to the calcineurin AB complex even with extensive dialysis against chelating agents (*12*). To identify this site and to gain further insights into the Ca^{2+}-binding properties of CnB, we prepared four single-site mutants designed to deactivate each Ca^{2+}-binding site in turn. Glu to Gln mutations were used, similar to those that have been shown to be effective in deactivating the Ca^{2+}-binding sites in calmodulin (*13*). Flow dialysis and metal analysis data were used to evaluate how many Ca^{2+} bind to the wild-type and each mutant form of the protein, and to determine the association constants for each site. Fourier transform infrared (FTIR) difference spectroscopy was also used to monitor effects of Ca^{2+} binding. The FTIR data support the conclusions of the Ca^{2+}-binding flow dialysis experiments with respect to the number of Ca^{2+} required to saturate each form of the protein. The FTIR data also suggest site 4 is the high-affinity Ca^{2+}-binding site. In addition, they provide information on the protein's secondary structure and changes that occur upon Ca^{2+} binding.

† This work was performed under the auspices of the Department of Energy under contract to the University of California and was supported by National Institutes of Health project (GM40528, J.T.).

* To whom correspondence should be addressed. Phone: (505) 667-2690. Fax: (505) 667-2891. E-mail: jtrewhella@lanl.gov.

‡ Laboratory of Biochemistry.

[1] Abbreviations: CnA, active site containing subunit of calcineurin; CnB, regulatory subunit of calcineurin; FTIR, Fourier Transform InfraRed spectroscopy.

10.1021/bi0025060 CCC: $20.00
Published on Web 09/15/2001

Table 1: Mutations in the Individual Ca^{2+}-Binding Sites of Calcineurin B

name	site mutated	mutagenic oligonucleotides[a]	mutation	restriction sites[b]
Q1 (Glu41Gln)	1	5′-CTGGTTCTTTGAGTGTGGAA**cAG** TTCATGagTCTGCCTGAGTTACAACAGA-3′	GAG→CAG	+*Bsp*HI
Q2 (Glu73Gln)	2	5′-GATGGGAATGGAGAAGTAGAtTTTAAA**cAA** TTCATTGAGGGCGTCTCT-3′	GAA→CAA	−*Acc*I, −*Eco*RI
Q3 (Glu110Gln)	3	5′-ATGGCTATATTTCCAATGGG**cAg**CTgTTCCAGGTAT TGAAGATGAT-3′	GAA→CAG	+*Pvu*II
Q4 (Glu151Gln)	4	5′-GGAGATGGAAGAATATCCTTcGAA**cAA** TTCAAAGCTGTTGTAGGT-3′	GAA→CAA	+*Bst*BI

[a] Replaced bases are shown by lower case letters, Gln codons are shown in bold characters and underlined. [b] (+) Added sites; (−) deleted sites.

MATERIALS AND METHODS

Mutagenesis. Restriction enzymes, ligations, DNA gel electrophoresis, and other recombinant DNA techniques were performed essentially as described by Sambrook et al. (*14*). The Altered Sites II-Ex1 *in vitro* Mutagenesis System was from Promega and the oligonucleotides were purchased from Genosys (Texas). The plasmid pBAKE carrying the coding region of human CnB was used to create the four CnB mutants using the Altered Sites II-Ex1 *in vitro* Mutagenesis System. The DNA fragment containing the entire coding sequence of CnB was excised by digestion with *Nco*I and *Bam*H1 and subcloned into the pAlter−Ex1 vector converted to ampicillin resistance by inclusion of an ampicillin repair oligonucleotide in the mutation reaction according to the manufacturer's instructions. Shown in Table 1 are the 5′-phosphorylated mutagenic oligonucleotides with the silent mutations introduced to create or omit specific restriction sites to facilitate mutant selection. ES1301 muS cells were transformed with the heteroduplex DNA and the transformants selected on LB plates containing 12.5 mg of ampicillin/mL. The coding sequence, excised with *Nco*I and *Bam*H1, were subcloned in the pET-11d expression vector and the entire coding sequence of the four mutants verified by DNA sequencing using the Dye Terminator Cycle Sequencing kit and oligonucleotides corresponding to the T7 promoter, TAATACGACTATAGGGGAATTG, and the CnB cDNA sequence, GACAATTCTGGTTCTTTGAGTGTGGA, with an ABI PRISM 310 genetic analyzer.

Protein Preparations. All protein samples were prepared using the expression system described in Anglister et al. (*9*). After the phenyl-sepharose chromatography, the protein samples, concentrated to 7−13 mg/mL with a centriprep-10 Amicon concentrator, were passed through two successive Pharmacia PD10 columns equilibrated with 20 mM HEPES-KOH buffer, pH 7.2, 0.1 M KCl, to remove EGTA. Ca^{2+} was removed from the samples by treatment with up to 2 mL/mg of protein prewashed Chelex-100. Residual Ca^{2+} was determined by atomic absorption spectroscopy. The molar ratio of Ca^{2+} to protein was 0.6, 0.2, 0.2, 0.1, and 0.1 for the wild-type CnB, Q1, Q2, Q3, and Q4 mutants, respectively. Protein concentrations for the decalcified proteins in 20 mM HEPES, pH 7.2, and 100 mM KCl were determined using an extinction coefficient at 276 nm of 4400 ± 100 based on protein concentrations measured in 6 M guanidine according to Edelhoch (*15*). The recombinant protein used for all studies in this paper is nonmyristylated and has Cys11 and Cys153 substituted by Ala and Lys, respectively, to avoid possible aggregation via disulfide bond formation. This recombinant protein has four Ca^{2+}-binding sites with the same structure as the wild-type protein (*9*) and, in this report, therefore, will be referred to as "wild-type." Additional mutations were done to sequentially inactivate each of the Ca^{2+}-binding sites. The substitutions were Glu-Gln in the Ca^{2+}-binding sites (Table 1, Figure 1). These substitutions have been shown to prevent Ca^{2+} binding in calmodulin (*13*). The amino acid sequence for CnB is shown in Figure 1 with its four Ca^{2+}-binding sites labeled 1−4 in order of their appearance (N- to C-terminus). The residues that contribute oxygen ligands to the Ca^{2+}-binding site are shown in bold. The four single-site mutants each have the last glutamate residue in the sequence of one of the binding sites replaced by a glutamine and are designated Q1 (=Glu41Gln), Q2 (=Glu73Gln), Q3 (=Glu110Gln), and Q4 (=Glu151Gln).

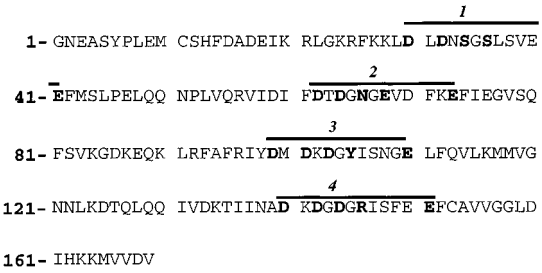

FIGURE 1: Amino acid sequence for human calcineurin B showing the Ca^{2+}-binding sites and the Ca^{2+} ligands. The Ca^{2+}-binding sites are indicated by the horizontal lines while the residues that coordinate Ca^{2+} are shown in bold. The mutants Q1 through Q4 have Gln substitutions for the last coordinating Glu in each site, i.e., Glu41Gln, Glu73Gln, Glu110Gln, and Glu151Gln, respectively. Note that for the experiments described in this paper the "wild-type" protein, CnB, and each mutant had the double mutation Cys11Ala, Cys153Leu to eliminate possible problems from intermolecular disulfide bond formation.

Ca^{2+} Binding by Flow Dialysis. Ca^{2+}-binding determinations were performed using the flow dialysis procedure (*16*) as described previously (*17*) except that the data were corrected for the loss of $^{45}Ca^{2+}$ (10−20%) from the well during the experiments (*12*). To accurately quantititate Ca^{2+} binding to the high-affinity sites of the wild-type and the Q1 and Q2 mutants, $^{45}Ca^{2+}$ was allowed to exchange with endogenous Ca^{2+} overnight at 0−4 °C prior to the flow dialysis experiment. Interval times between collecting samples after each addition of Ca^{2+} for determination of free Ca^{2+} were chosen to maximize exchange of free and bound Ca^{2+} (2−3.2 min). Final free Ca^{2+} concentrations were 0.9 mM.

FTIR Experiments. FTIR experiments were done using protein samples in D_2O with 25 mM HEPES, pH 7.9 (uncorrected meter reading), and 100 mM KCl. The decalcified proteins were dialyzed twice against 100 vol of D_2O (<0.08 μM Ca^{2+}) in the presence of 5 mL of chelex-100 resin (Biorad)/50 mL of D_2O. Plasticware and dialysis tubing

had been washed free of Ca^{2+} as previously described (*18*). The samples were then lyophilized for storage and taken up (to ~10 mg/mL) in the HEPES buffer immediately prior to the FTIR experiments. Protein concentrations were 5−20 mg/mL. The buffer used to dissolve the lyophilized protein had a small amount of Chelex-100 resin (Bio-Rad) added to take up any Ca^{2+} that might have entered the system by leaching from the sample containers, for example. The resin was removed prior to FTIR measurement by gentle centrifugation (1500*g*). Ca^{2+} titrations were done by addition of $CaCl_2$.

FTIR spectra were measured at 2 cm^{-1} resolution using a Bio-Rad FTS 40 FTIR spectrometer. For each spectrum, 1024 scans were co-added to improve the signal-to-noise ratio. Sample cells had CaF_2 windows with an 0.05 mm Teflon spacer to fix the path length. Trewhella et al. (*19*) found previously that there is negligible leaching of Ca^{2+} from the windows within the ~2 h time frame of the FTIR experiments. The spectrometer optical bench was maintained under constant dry N_2 to reduce effects of water vapor in the spectra. Absorbance spectra for protein solutions were collected after a minimum of 30 min N_2 purge and the buffer contribution was removed by subtraction of a normalized buffer spectrum. The end points for each titration were repeated to ensure reproducibility of the results. FTIR spectra were analyzed as described in Trewhella et al. (*19*), except analysis of the deconvolved spectra was done using a "global curve fitting analysis" that fits a set of similar spectra simultaneously. The analysis uses either Gaussian or Lorentzian functions to determine peak positions and areas for bands under the spectral envelope (*20*). We used this approach previously in the analysis of FTIR spectra from calmodulin and its complexes with sequence segments from the smooth muscle protein caldesmon (*21*).

Sedimentation Equilibrium Experiments. A Beckman Optima XL-A analytical centrifuge with a four position An-Ti rotor was used for the sedimentation equilibrium experiments. The partial specific volume of calcineurin B (0.716 mL g^{-1}) was calculated according to Zamyatnin (*22*). Solutions of wild-type CnB in 10 mM HEPES, pH 7.5, 0.1 M KCl and 0.5 mM Ca^{2+} or 2 mM EGTA (0.1 mL) and 0.12 mL of the corresponding buffers were loaded on the right and left sides, respectively, of a double sector 1.2 cm six-channel cell. After equilibrium for 1 h at 3000 rpm and 20 °C, the rotor was accelerated to 15 000 rpm, and after 45 h, equilibrium was monitored by scanning the cells every 4 h. The data were analyzed using extinction coefficients at 280 nm of 4500 ± 100 in the presence of Ca^{2+} and 4300 ± 100 in the presence of EGTA based on protein concentration determined in 6 M GuHCl (*15*) and the data analysis software from Beckman (Palo Alto, California).

RESULTS

Ca^{2+} Binding to Wild-Type CnB and the Mutants Measured by Flow Dialysis. Figure 2, panels a and b, show the Ca^{2+}-binding data measured by flow dialysis for the wild-type CnB and the four mutants, Q1 through Q4. The lines are the computer-derived fits of the experimental points to the Adair-Klotz equation (*23*). These data give the number of bound Ca^{2+} for each protein as a function of free Ca^{2+} concentration. Each binding experiment was done at least two times to ensure reproducibility. As expected, the wild-type CnB saturates at 4 Ca^{2+}/mol of protein while mutants Q1, Q3, and Q4 appear to saturate at three and Q2 at 2 Ca^{2+}/mol of protein.

Table 2: Macroscopic Binding Constants of the Wild-Type CnB and Mutants

	N	K_1	K_2	K_3	K_4	j	RSD
wild-type	0.9	11	81	0.15	0.03	0.0019	0.17
wild-type (with Mg^{2+})[a]	0.9	4	4	0.26	0.07	0.0017	0.13
Q1	0.9	15	49		0.02	0.0030	0.10
Q2	0.9	2	12			0.0030	0.12
Q3	1.1	0.6		0.06	0.01	0.0016	0.10
Q4	1.0	0.5		0.23	0.01	0.0012	0.06

[a] Experiments done in the presence of 1 mM $Mg^{2+}Cl_2$. Macroscopic association constants K_1, K_2, K_3, and K_4 (μM^{-1}) were determined by fitting the data to the Adair-Klotz equation (*23*):

$$y = N\frac{(K_1x + 2K_1K_2x^2 + ... + nK_1...K_nx^n)}{(K_1x + K_1K_2x^2 + ... + K_1...K_nx^n)} + jx$$

where y = mol of bound Ca^{2+}/mol of CnB, x = free Ca^{2+} determined experimentally, n = the number of sites/mol CnB selected for the fit (4 for the wild-type protein and 3 for Q1, Q3, and Q4, and 2 for Q2), j is the slope term for nonspecific binding, and N is the ratio of the number of specific sites derived from fitting the data to the value of n used for the fit of the data to the above equation. RSD is the residual standard deviation.

The association constants derived by fitting the data to the Adair-Klotz equation (Table 2) reveal that the wild-type protein with its higher residual Ca^{2+} content (~0.6 equivalents) has two pairs of sites, one pair with very high affinities and the other with low affinities. Under our experimental conditions, the affinities of the high-affinity sites are similar in magnitude to the single high-affinity Ca^{2+} site of CnB reported by Kakalis et al. (*24*). Failure to identify a second high-affinity site in this study may have been due to different experimental conditions (they used myristylated calcineurin B in 0.2 M KCl). The identification of two pairs of Eu^{3+}-binding sites in unmyristylated calcineurin B, one with high affinity (dissociation constants, K_d, of 0.14 and 0.020 μM) and one with 10−100-fold lower affinity (K_d values of 1 and 1.5 μM), led Burroughs et al. (*25*) to propose that the ion-binding properties of calcineurin B were more like troponin C (TnC) than calmodulin. Calcineurin B, with distinct structural and activation Ca^{2+} sites (reviewed in ref *1*), is also functionally more similar to TnC than to calmodulin. It is therefore not surprising that the high-affinity sites of calcineurin B, like those of TnC, are Mg^{2+}-binding sites and their affinity for Ca^{2+} is significantly decreased in the presence of 1 mM $MgCl_2$ (Table 2). Our binding data show that in the presence of Mg^{2+} there is a decrease in affinity for the high-affinity sites, whereas the low affinity sites are not significantly affected. There remains 1−2 orders of magnitude difference between the high- and low-affinity sites, however. These results are similar to those of Feng and Stemmer (*26*) who report Ca^{2+} affinities for CnB measured in the presence of 1 mM $Mg^{2+}Cl_2$.

Also, in agreement with the reduced affinity of the two high-affinity sites observed in the Glu110Lys and the Glu151Lys mutants of unmyristylated calcineurin B used by Feng and Stemmer (*26*), we observe (Figure 2a, Table 2) greatly decreased affinities in the Q3 and Q4 mutants, both of which can be fully decalcified (residual Ca^{2+} ~0.1 equiv). In contrast, the Q1 and Q2 mutants, with residual 0.2 Ca^{2+} equiv each, retain two apparently high-affinity sites (Figure

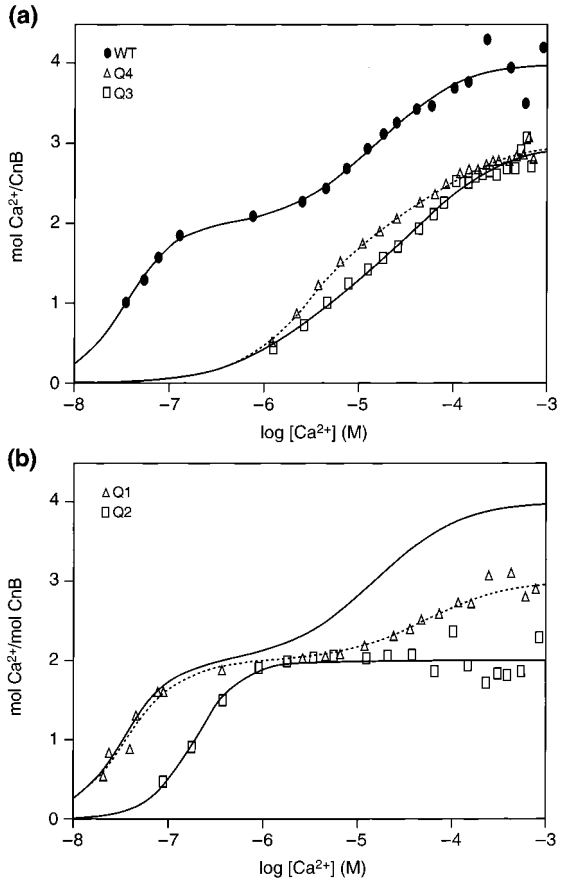

FIGURE 2: Ca^{2+}-binding data measured by flow dialysis. Ca^{2+} binding was determined in 10 mM HEPES, pH 7.5, 0.1 M KCl. Concentrations of the individual proteins were 20 μM for the wild-type CnB, 20 μM for Q1 and Q2, and 25 μM for Q3 and Q4. The lines show the computer derived fits of the experimental points to the Adair-Klotz equation using the binding constants listed in Table 2 after subtraction of nonspecific binding (jx) and correction for $N = 1$. (a) Binding data and computer-derived fits for wild-type CnB (filled circles) and mutants Q3 (open squares) and Q4 (open triangles). (b) Binding data and computer-derived fits for mutants Q1 (open triangles) and Q2 (open squares). The computer-derived fit for the wild-type CnB (Figure 1a) is shown for comparison.

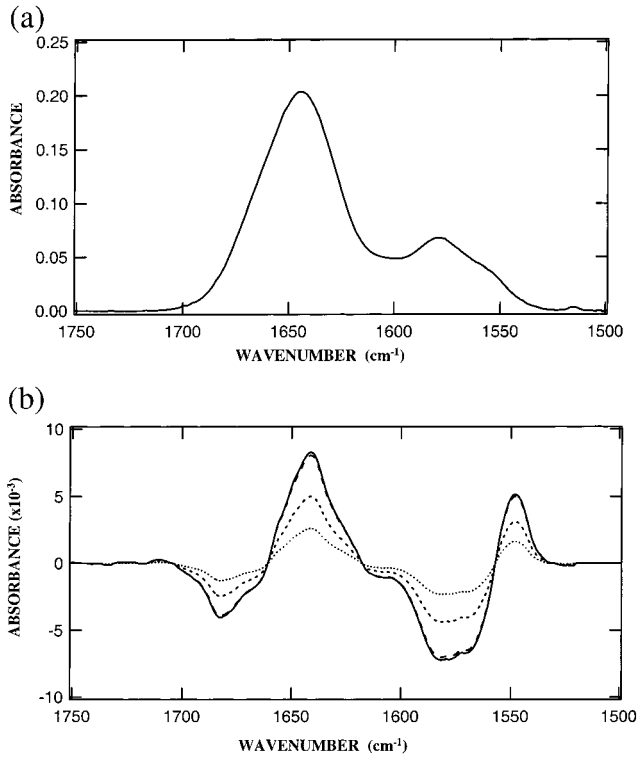

FIGURE 3: FTIR spectra for wild-type CnB. (a) The absorbance spectrum for CnB with one Ca^{2+} bound to the very high-affinity site. Contributions from the buffer were subtracted to give the spectrum due to the protein only. (b) The difference spectra calculated as the spectrum obtained upon each Ca^{2+} addition minus the spectrum for 1 Ca^{2+}/mol protein. Additions of 1 (dots), 2 (short dash), 3 (long dash), and 4 (solid) Ca^{2+} equiv thus correspond to 2, 3, 4, and 5 total Ca^{2+} equiv/mol protein.

2b, Table 2), as do the Glu41Lys and Glu73Lys mutants of Feng and Stemmer (*26*). In our experiments, Q1 and Q2 retain both high-affinity sites, but the affinity of these sites are somewhat reduced in Q2. It is therefore likely that the high-affinity sites are located in the C-domain of CnB. The greatly reduced affinity of a remaining high-affinity site in the Q3 and Q4 mutants indicates that integrity of either one of these sites is required for the high affinity of the other. Moreover, a significant decrease in affinity for the two high-affinity sites was observed in the Q2 mutant, whereas Q3 shows decreased affinities for two low-affinity sites. Taken together, these data indicate that, within each pair of sites, a mutation in one site reduces the affinity of the other, and mutations in sites 2 and 3 also affect the affinity of the sites in opposite lobes of CnB. Thus, different substitutions may have different effects on the structure of the proteins but the data are all consistent with the existence of communication between the four sites of CnB.

Ca^{2+} Titration of Wild-Type CnB and the Mutants Monitored by FTIR Spectroscopy. Overall Features of the FTIR Spectra. Figure 3a shows the absorbance spectrum for wild-type CnB. The same broad features, with maxima at 1642 and 1583 cm^{-1}, are seen in the spectra of the wild-type and each mutant protein. The broad peak centered at 1642 cm^{-1} is dominated by the carbonyl stretching frequencies of the polypeptide backbone and is generally referred to as the amide I′ band. The designation I′ is used for proteins solubilized in D_2O which results in small shifts to lower values of the carbonyl stretching frequencies compared to proteins in H_2O. The components in the amide I′ band are sensitive to the chemical environment of the carbonyl bonds and to the secondary structural elements they participate in ref *27* or their ligation state. The smaller broad peak centered at 1583 cm^{-1} is attributed to the asymmetric stretching frequency of carboxylate groups ($-COO^-$)in the protein (*27, 28*). This latter region of the spectrum is where we expect to see changes as the Glu and Asp ligands coordinate Ca^{2+}.

Assignment of Changes in Carboxylate Regions Due to Ca^{2+} Coordination of Carboxylate Groups. Figure 4 summarizes the 7-coordinate Ca^{2+} sites in the N- (Figure 4a) and C-domain (Figure 4b) of calcineurin B based on the crystal structure of the calcineurin/FKBP12-FK506 complex (*7*). All four sites have the Ca^{2+} coordinating with one water molecule and the carboxylate side chains of one Glu (bidentate) and two Asp residues (monodentate). The sites in the N-domain then have either Asn (site 1) or Ser (site 2) and the carbonyl of either Ser (site 1) or Glu (site 2). The C-domain sites have an additional Asp and the carbonyl of either a Tyr (site 3) or an Arg (site 4). The additional Asp

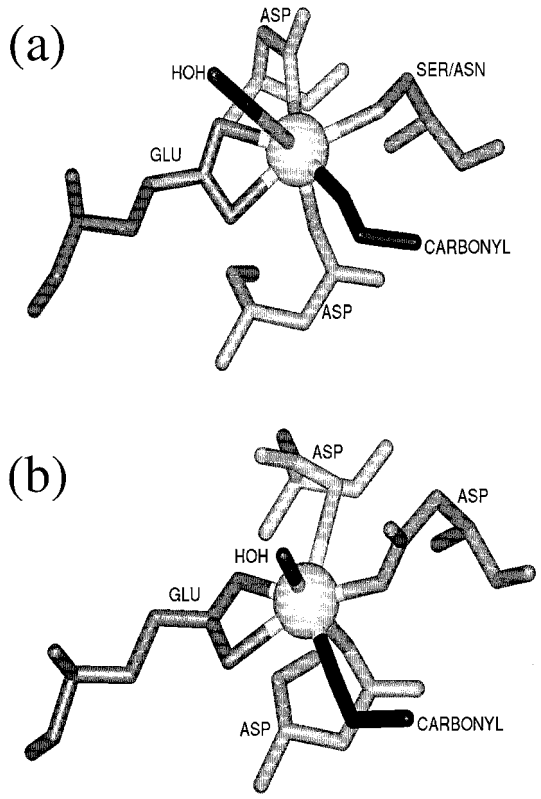

FIGURE 4: Schematic representation of the Ca^{2+}-binding ligands. (a) Ca^{2+} ligands for N-domain Ca^{2+}-binding sites. In site 2, the Ser residue in site 1 is replaced by Asn. (b) Ca^{2+} ligands for C-domain Ca^{2+}-binding sites. The residues providing a backbone carbonyl ligand are Ser36, Glu68, Tyr105, and Arg146 for sites 1 through 4, respectively.

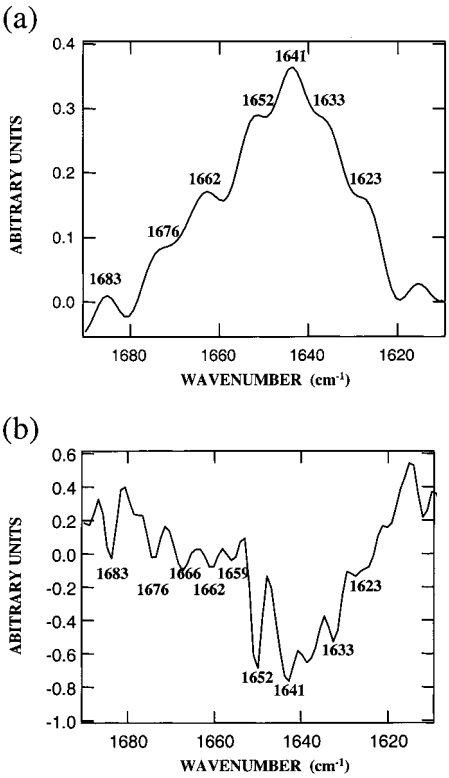

FIGURE 5: (a) Fourier-deconvolved amide I′ band of the wild-type CnB. (b) Second derivative spectrum of the wild-type CnB.

residues in sites 3 and 4 likely would give rise to higher Ca^{2+} affinities for these sites compared to sites 1 and 2. The changes in absorption observed in the difference spectra for CnB at 1570 and 1585 cm^{-1} are assigned to carboxylate asymmetric stretching frequencies of delocalized Asp and Glu residues (*28*).

When the carboxylate groups coordinate Ca^{2+}, there is a shift in frequency of the C−O stretch. Bidentate coordination results in a shift to lower frequency by ∼25 cm^{-1} while monodentate coordination results in a shift to higher frequency by ∼35 cm^{-1} (*29*). Upon Ca^{2+} titration, the spectra for the wild-type and mutant forms each show a gain in intensity at 1545 cm^{-1} accompanying the losses of intensity at 1570 and 1585 cm^{-1} (see below). There are also contributions to changes around 1600−1620 cm^{-1}, although overlap with the amide I′ region (1690−1625 cm^{-1}) makes that difficult to resolve. We therefore assign the 1545 cm^{-1} band to the carboxylate of the Glu side chains having bidentate coordination to Ca^{2+} and some proportion of the contributions at ∼1620 cm^{-1} to the carboxylate of the Asp side chain with monodentate coordination to Ca^{2+}.

Assignment of Changes in Amide I′ Bands to Secondary Structure Changes. Figure 5a shows a deconvolution of the absorption spectrum in Figure 3a, while Figure 5b shows the corresponding second derivative spectrum. The enhanced resolution obtained following deconvolution (*30*) or by taking the second derivative (*31*) of an FTIR spectrum allows for the assignment of specific peaks in the amide I′ band to secondary structure elements (*27*). Importantly, essentially the same features are seen in both the deconvolution and second derivative calculations from the spectra of the wild-type CnB and mutant proteins. Further, the wild-type and mutant proteins each show the same general features. In the amide I′ region, bands are observed at 1623, 1633, 1641, 1652, 1666, 1676, and 1683 cm^{-1}. The bands at 1623, 1633, and 1676 cm^{-1} are assigned to the low- and high-frequency components of extended chain. The 1683 and 1666 cm^{-1} bands are assigned to turns or bends. The latter band is seen in the second derivative spectrum with two additional features at 1669 and 1659 cm^{-1} that also lie in the turns or bends region. These differences likely reflect the difficulty of resolving small bands in noisy spectra. The 1652 cm^{-1} band is assigned to α-helix, while that at 1641 cm^{-1} is associated with random structure. Alternatively, the 1641 cm^{-1} band can be assigned to solvent exposed helix in which the carbonyl backbones within the helix participate in double hydrogen bonds involving the normal α-helix scheme plus a water molecule (*32*). Evidence for a high proportion of solvated helix has previously been observed in FTIR spectra for calmodulin and troponin C (*19*). Table 3 gives the intensities of the amide I′ bands relative to the total amide I′ intensity for the wild-type CnB and mutants, at each Ca^{2+} concentration. These intensities were derived from the global curve-fitting analysis of the deconvolved spectra (see Materials and Methods). The percentage helical structure obtained from the FTIR measurements of the wild-type Ca^{2+} saturated protein is identical to that determined by NMR for Ca^{2+}-saturated calcineurin B in solution (*9*).

Analysis of the Spectral Changes upon Ca^{2+} Titration. Difference FTIR spectra of the wild-type protein (Figure 3b) and the four mutants (Figures 6 and 7) were calculated as subtractions of the spectra measured for the protein with no

Table 3: Contributions to the Amide I′ Band[a]

protein	relative intensity of bands (at frequencies in cm^{-1}) in amide I′ region (%) 0 Ca^{2+} added/4 equivalents Ca^{2+} added						
	1623 cm^{-1}	1633 cm^{-1}	1641 cm^{-1}	1652 cm^{-1}	1666 cm^{-1}	1676 cm^{-1}	1683 cm^{-1}
wild-type	2/3	9/8	30/34	48/48	4/4	2/2	5/1
Q1	3/2	9/8	30/30	49/53	4/4	2/1	5/2
Q2	2/3	10/9	30/32	48/48	4/3	2/2	4/3
Q3	2/2	10/10	30/34	48/47	4/4	2/2	4/1
Q4	3/3	10/10	29/33	48/47	3/4	2/2	5/1

[a] The percentage values given are calculated as the relative intensities of bands under the amide I′ envelope calculated using a global curve fitting analysis (*20*).

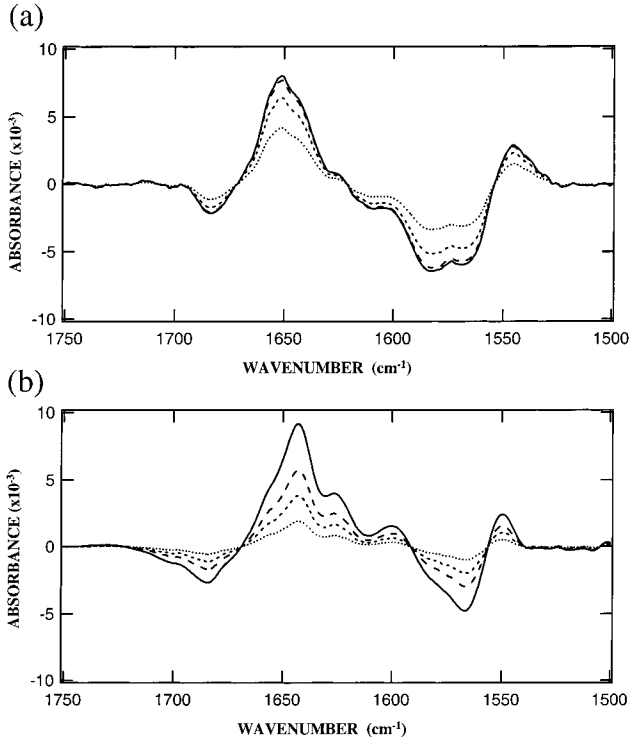

FIGURE 6: Ca^{2+} titration difference spectra for the two N-domain mutants (Q1, Q2). (a) The difference spectra calculated by subtracting the spectrum obtained upon each Ca^{2+} addition minus the apo-Q1 spectrum. The key for the Ca^{2+} additions is 1 (dots), 2 (short dash), 3 (long dash), and 4 (solid) equiv/mol of protein. (b) The difference spectra calculated by subtracting the spectrum obtained upon each Ca^{2+} addition minus the apo-Q2 spectrum. The key for the Ca^{2+} additions is 1 (dots), 2 (short dash), 4 (long dash), and 10 (solid) equiv/mol of protein.

added Ca^{2+} from the spectrum obtained upon each Ca^{2+} addition. Each Ca^{2+} titration was repeated a minimum of three times to ensure reproducibility. To facilitate comparison between different protein samples, all spectra were normalized to integrated intensity under the amide I′ band. In the difference spectra for each form of the protein, we observe progressive changes in the amide I′ region with increasing Ca^{2+}. For the wild-type, Q2, Q3, and Q4 proteins there is a loss of absorbance intensity at 1683 cm^{-1} and an accompanying increase in intensity at 1641 cm^{-1}. For Q1 this increase is observed at the higher frequency of 1652 cm^{-1}. These differences might be attributable to small differences in solvated helix between Q1 and the other mutants and wild-type CnB. Changes are also observed in the carboxylate

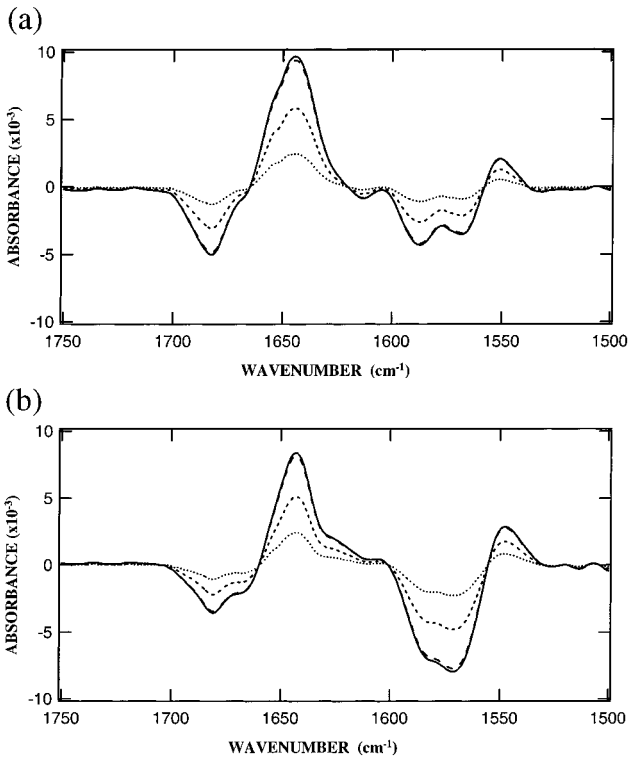

FIGURE 7: Ca^{2+} titration difference spectra for the two C-domain mutants (Q3, Q4). The difference spectra obtained by subtracting the spectrum obtained upon each Ca^{2+} addition from that for the apo-forms of the (a) Q3 and (b) Q4 mutants. The same key for Ca^{2+} addition is as for Figure 6a; 1 (dots), 2 (short dash), 3 (long dash), and 4 (solid) equiv/mol of protein.

Table 4: Changes in the Carboxylate Region of the FTIR Spectra as a Function of Ca^{2+} Content Given as a Percentage of the Total Change Observed for Wild-Type CnB and the Mutants with 10 equiv of Ca^{2+} Added[a]

protein	carboxylate stretching frequency (cm^{-1})	equivalents of Ca^{2+} added			
		1	2	3	4
wild-type	1570	32	60	96	101
	1585	30	62	97	101
Q1	1570	52	81	93	99
	1585	51	78	92	99
Q2	1570	20	31	-	61
	1585	21	38	-	62
Q3	1570	24	62	98	100
	1585	25	65	101	100
Q4	1570	29	61	96	100
	1585	29	60	97	100

[a] The percentages are calculated using the results of the global curve fitting analysis (*20*) on the deconvolved spectra for the Ca^{2+} titration of the wild type and mutant proteins.

region of the spectrum due to Ca^{2+} coordinating to the protein. There is a decrease in intensity at the frequencies assigned to unligated Glu and Asp residues (1570, 1585 cm^{-1}, respectively), and an increase at the frequencies assigned to bidentate Glu ligands (1545 cm^{-1}) in all forms of the protein. The carboxylate region is most sensitive to the details of Ca^{2+} ligation at each site and these bands are well resolved. It is therefore useful to quantitate the changes in this region in terms of the percent change of the total for each point in the titration using the results of the global curve fitting analysis (Table 4).

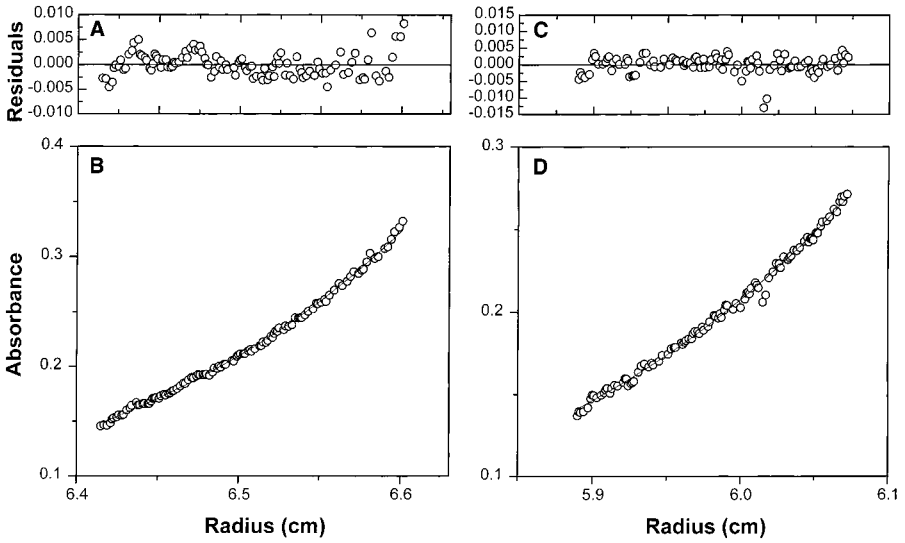

FIGURE 8: Sedimentation equilibrium experiment for wild-type CnB. Protein concentration is 0.9 mg/mL, 20 °C and 15 000 rpm in the presence of 10 mM HEPES, pH 7.5, 0.1 M KCl, as well as 0.5 nM Ca^{2+} (panels A and B) or 2 mM EGTA (panels C and D). The absorption data at 280 nm (B and D, open circles) are shown together with a model fit assuming a 19 163 molecular weight and a monomer−dimer equilibrium (solid line). The residual ($A_{exp} - A_{model}$) is shown in panels A and C.

Consistent with the Ca^{2+}-binding data, the spectral changes for the wild-type protein, Q1, Q3, and Q4 are complete upon addition of 3 equiv of Ca^{2+}, whereas Q2 is only about half saturated with 4 equiv of Ca^{2+}. For the wild-type protein (Figure 3b, Table 4), with its one very high-affinity site already occupied, the spectral changes for each equivalent of Ca^{2+} added are approximately equal and ~96−97% of the total change is complete upon addition of three equivalents of Ca^{2+}. The difference spectra of the N-domain mutants Q1 and Q2 (Figure 6) are distinct from each other, as well as from the wild-type and the C-domain mutants. Addition of the first 2 equiv of Ca^{2+} to Q1 accounts for ~50 and ~80% of the total spectral changes (Table 4), respectively. This nonlinear response indicates that the available Ca^{2+}-binding sites do not all give rise to equivalent spectral changes, and that they fill in some order. This result is consistent with two high-affinity Ca^{2+} sites being retained in the Q1 mutant. The N-domain mutant, Q2, shows a slower rate of change in absorbance as a function of Ca^{2+} concentration compared to all the other forms, and the changes are not complete even with addition of 10 equiv of Ca^{2+} (data not shown). Only ~60% of the total observed spectral change is seen with 4 equiv of Ca^{2+}/mol of protein. This result is also consistent with the Ca^{2+}-binding data and indicates that loss of site 2 in the N-domain lowers the Ca^{2+} affinity at two of the remaining three sites, which includes at least one in the C-domain.

Similar to the wild-type protein, the difference spectra for the C-domain CnB mutants, Q3 and Q4, show approximately equal spectral changes upon addition of each Ca^{2+} up to 3 equiv added (Figure 7, Table 4). The magnitude of the total change observed in the amide I′ region is very similar for wild-type, Q3, and Q4 mutants. In contrast, the magnitude of the changes observed in the carboxylate region of Q3 is much smaller (about half) than those seen for wild-type CnB and for Q4 (Table 4). The similarity of the Ca^{2+}-induced differences observed for wild-type and Q4 suggests that the same three sites are titrated in these proteins. In other words, under the conditions of the FTIR experiments, the very high-affinity site that cannot be decalcified in the wild-type protein appears to be site 4.

The changes in the intensities of bands under the amide I′ envelope determined using the global curve fitting analysis (Table 3) are in excellent agreement with the difference spectra. The largest effects in the amide I′ region due to Ca^{2+} binding to the wild-type protein is seen in the 1641 (random structure or solvent exposed helix) and 1683 (turns or bends) cm^{-1} bands (Table 3, Figure 3b). The global curve fitting analysis indicates that upon Ca^{2+} binding to wild-type CnB there is a 4% loss of intensity in the region assigned to turns or bends and a corresponding 4% gain in the region assigned to random structure or perhaps solvated helix. A 4% change in the amide I′ intensity translates into a change involving ~7 residues. Three of these seven residues showing changes might be those with backbone carbonyl groups involved in Ca^{2+} ligation at each of the Ca^{2+} sites being titrated. We cannot tell with the present data, therefore, whether ~4 or ~7 residues are involved in changes due to secondary structural rearrangements. Consistent with the difference spectra, the changes observed in the distribution of intensities under the amide I′ band for the Q3 and Q4 mutants upon Ca^{2+} titration are indistinguishable from those observed for the wild-type CnB. Likewise, the Q2 mutant shows changes at 1683 and 1641 cm^{-1} in the same direction as for wild-type but they are smaller by about one-half, also consistent with the difference spectra for Q2. The Q1 mutant shows similar changes in magnitude and direction to the wild-type protein, but the positive change is at the ideal α-helix band at 1652 instead of 1641 cm^{-1}. Again the difference spectrum shows the same effects, with the 1683 cm^{-1} difference intensity somewhat suppressed because it more strongly overlaps with the positive difference peak at 1652 cm^{-1} (compared with 1641 cm^{-1}).

Protein Dimerization Effects. Under the conditions used in our FTIR and binding experiments, wild-type CnB dimerizes with an equilibrium constant measured as $(8.0 \pm 0.8) \times 10^{-4}$ M in the presence of EGTA and $(3.0 \pm 0.2) \times 10^{-4}$ M in the presence of Ca^{2+} (Figure 8). At the pro-

tein concentrations used for the flow dialysis experiments (20−25 μM) 11.0 ± 0.5% (with Ca^{2+}) or 5 ± 0.5% (with EGTA) of the protein will be dimerized. This type of Ca^{2+}-dependent dimerization seen in calcineurin B is also observed in the structurally and functionally related troponin C. It is the result of a Ca^{2+}-induced change in solvent accessibility of hydrophobic residues in the protein (*33*, *34*). The good fit of our binding data for the wild-type CnB in the presence of Ca^{2+} to four sites with an RSD of 0.17 (Table 2) suggests that the concentration of dimer in this sample is too low to detect any effects on the Ca^{2+} binding. However, a precise determination of the Ca^{2+}-binding constants for CnB (and for the mutants) should take into account effects of Ca^{2+}-dependent dimerization of the protein. Because wild-type CnB has four Ca^{2+}-binding sites, such a study requires the determination of dimerization constants for the wild-type (and each mutant) protein at different concentrations of Ca^{2+}, as well as Mg^{2+}. We have begun such a study and the results will be key to establishing the mechanism for the observed communication between sites. That is, whether the communication is mediated by dimerization effects or if the communication is a property of the individual protein monomer.

The FTIR studies were done at concentrations where we expect the protein to be composed almost entirely of dimers. To assess possible impact of dimerization on our FTIR results, we therefore collected data for the protein in 25 mM CHAPS. NMR experiments have shown that 25 mM CHAPS inhibits CnB dimerization (*35*) at the high concentrations needed for these experiments. This effect is due to the detergent-like properties of CHAPS that enable it to disrupt hydrophobic interactions between the proteins. FTIR spectra were acquired for the apo wild-type CnB in CHAPS buffer, as well as the Ca^{2+} saturated state, by addition of $CaCl_2$ (data not shown). The same spectral changes were observed as in the experiments in HEPES buffer.

CONCLUSIONS

The Ca^{2+}-binding data from our flow dialysis and FTIR experiments show that wild-type CnB as well as the Q1, Q3, and Q4 mutants each require 3 equiv of Ca^{2+} to saturate. In the case of the wild-type protein, the binding data show that it cannot be decalcified and always retains one bound Ca^{2+} leaving only three sites available for titration. The binding data reveal two pairs of sites in the wild-type protein, one pair with unusually high affinity and one pair with low affinity. Because the C-domain Ca^{2+}-binding sites have an additional coordinating Asp (instead of a Ser or Asn) we expect that the high-affinity sites are in the C-domain. The fact that the Q1 mutant retains two high-affinity sites is consistent with this expectation. The strong similarity between the FTIR spectral changes upon Ca^{2+} binding observed for the wild-type protein and Q4 suggests that the same three sites are titrated in these proteins. That is, under the conditions of the FITR experiments, site 4 is the high-affinity site in the wild-type CnB that cannot be decalcified.

The differences in association constants between the high- and low-affinity sites for the wild-type CnB are 1−3 orders of magnitude, and lead one to conclude that calcineurin B with its distinctive high-affinity structural and lower affinity regulatory Ca^{2+}-binding sites is like troponin C. In contrast, calmodulin's four Ca^{2+}-binding sites differ in binding affinity by less than 1 order of magnitude although there is evidence that target enzyme binding to calmodulin increases these differences (*36*−*38*).

The binding and FTIR data indicate that mutation of any one of the Ca^{2+}-binding sites in CnB affects the affinity at other sites. In other words, there is communication between the sites, both within each globular domain and between the N- and C-domains. For example, mutation of any one of the N- or C-domain sites lowers the affinity of the site that cannot be decalcified in the wild-type protein. Further, the N-domain mutant Q2 lowers the affinity of two of the remaining sites, one of which has to be in the C-domain. Communication between the two domains of CnB could be mediated by the mostly helical region that connects the N- and C-domains. The helical segments either side of the flexible segment at Gly85 each become one of the helices in the EF-hands that form Ca^{2+}-binding sites 2 and 3. An alternative mechanism that we are currently exploring is the possibility of the communication arising from dimer formation.

ACKNOWLEDGMENT

We thank James Bailey and Feng Gai for help with the FTIR instrumentation, data reduction, and analysis tools, and Ren Hao for advice in performing the mutagenesis experiments. We thank Sergei Ruvinov for performing the sedimentation equilibrium experiments and Xutong Wang for preliminary Ca^{2+}-binding studies.

REFERENCES

1. Klee, C. B., Ren, H., and Wang, X. (1998) *J. Biol. Chem. 273*, 13367−13370.
2. Liu, J., Farmer, J. D., Jr., Lane, W. S., Friedman, J., Wiessman, I., and Schreiber, S. L. (1991) *Cell 66*, 807−815.
3. Liu, J., Albers, M. W., Wandless, T. J., Luan, S., Alberg, D. G., Belshaw, P. J., Cohen, P., MacKintosh, C., Klee, C. B., and Scrieber, S. L. (1992) *Biochemistry 31*, 3896−3901.
4. Schreiber, S. L., and Crabtree, G. R. (1993) *Immunol. Today 13*, 136−142.
5. Schreiber, S. L. Albers, M. W., and Brown, E. J. (1993) *Acc. Chem. Res. 26*, 136−142.
6. Aitken, A., Klee, C. B., and Cohen, P. (1984) *Eur. J. Biochem. 139*, 663−671.
7. Griffith, J. P., Kim, J. L., Kim, E. E., Sintchak, M. D., Thomson, J. A., Fitzgibbon, M. J., Fleming, M. A., Caron, P. R., Hsiao, K., and Navia, M. A. (1995) *Cell 82*, 507−522.
8. Kissinger, C. R., Parge, H. E., Knighton, D. R., Lewis, C. T., Pelletier, L. A., Tempczyk, A., Kalish, V. J., Tucker, K. D., Showalter, R. E., Moomaw, E. W., Gastinel, L. N., Habuka, N., Chen, X., Maldonado, F., Barker, J. E., Bacquet, R., and Villafranca, E. (1995) *Nature 378*, 641−644.
9. Anglister, J., Grzesiek, S., Wang, A. C., Ren, H., Klee, C. B., and Bax, A. (1994) *Biochemistry 33*, 3540−3547.
10. Ikura, M., Spera, S., Barbato, G., Kay, L. E., Krinks, M., and Bax, A. (1991) *Biochemistry 30*, 9216−9228.
11. Barbato, G., Ikura, M., Kay, L., Pastor, R., and Bax, A. (1992) *Biochemistry 31*, 5269−5278.
12. Stemmer, P. M., and Klee, C. B. (1994) *Biochemistry 33*, 6859−6866.
13. Maune, J. F., Klee, C. B., Beckingham, K. (1992) *J. Biol. Chem. 267*, 5286−5295.
14. Sambrook, J., Fritsch, E. F., and Maniatis, T. (1989) *Molecular Cloning: A Laboratory Manual*, 2nd ed., Cold Spring Harbor Laboratory, Plainview, NY.
15. Edelhoch, H. (1967) *Biochemistry 6*, 1948−1954.
16. Colowick, S. P., and Womack, F. C. (1960) *J. Biol. Chem. 244*, 774−777.

17. Haiech, J., Klee, C. B., and Damaille, J. G. (1981) *Biochemistry 20*, 3890−3897.
18. Crouch, T. H., and Klee, C. B. (1980) *Biochemistry 19*, 3692−3698.
19. Trewhella, J., Liddle, W. K., Heidorn, D, B., and Strynadka, N. (1989) *Biochemistry 28*, 1294−1301.
20. VanStokkum, I. H. M, Linsdell, H., Hadden, J. M., Haris, O. I., Chapman, D., and Blomendal, M. (1995) *Biochemistry 34*, 10508−10518.
21. Krueger, J. K., Gallagher, S. C., Wang, C.-L. and Trewhella, J. (2000) *Biochemistry 39*, 3979−3987.
22. Zamyatnin, A. A. (1984) *Annu. Rev. Biophys. Bioeng. 13*, 145−165.
23. Fletcher, J. E., Spector, A. A., and Ashbrook, J. D. (1970) *Biochemistry 9*, 4580−4587.
24. Kakalis, L. T., Kennedy, M., Sikkink, R., Rusnak, F., and Armitage, I. M. (1995) *FEBS Lett. 362*, 352−355.
25. Burroughs, S. E., Horrocks, W. D., Jr., Ren, H., and Klee, C. B. (1994) *Biochemistry 33*, 10428−10436.
26. Feng, B., and Stemmer, P. M. (1999) *Biochemistry 38*, 12481−12489.
27. Byler, D. M., and Susi, H. (1986) *Biopolymers 25*, 469−487.
28. Venyaminov, S. Y., and Kalnin, N. N. (1990) *Biopolymers 30*, 1243−1257.
29. Nara, M., Torjii, H., and Tasumi, M. (1996) *J. Phys. Chem. 100*, 19812−19817.
30. Kauppinen, J. K., Moffatt, D. J., Mantsch, H. H., and Cameron, D. C. (1981) *Appl. Spectrosc. 35*, 271−276.
31. Cameron, D. G., and Moffatt, D. J. (1987) *Appl. Spectrosc. 41*, 539−544.
32. Parrish, J. R., and Blout, E. R. (1972) *Biopolymers 11*, 1001.
33. Herzberg, O., and James, M. N. G. (1985) *Nature 313*, 653−659.
34. Blechner, S. L., Olah, G. A., Strynadka, N. C. J., Hodges, R. S., and Trewhella, J. (1992) *Biochemistry 31*, 11326−11334.
35. Anglister, J., Grzesiek, S., Wang, A. C., Ren, H., Klee, C. B., and Bax, A. (1993) *J. Biomol. NMR 3*, 121−126.
36. Bayley, P., Findlay, W. A., and Martin, S. R. (1996) *Protein Sci. 5*, 1215−1228.
37. Johnson, D. J., Snyder, C., Walsh, M., and Flynn, M. (1996) *J. Biol. Chem. 271*, 761−767.
38. Peerson, O. B., Madsen, T. S., and Falke, J. J. (1997) *Proteins Sci. 6*, 794−807.

BI0025060